Geophys. J. R. astr. Soc. (1972) **31**, 83–97.

Source Time Functions and Spectra for Underground Nuclear Explosions

David von Seggern and Robert Blandford

(Received 1972 August 13)*

Summary

The model of Haskell for explosion source time functions and spectra fails to satisfy data in the short-period band recorded teleseismically from the three Amchitka Island underground nuclear tests: LONGSHOT, MILROW, and CANNIKIN. A more recent model due to Mueller and Murphy satisfies the data quite well. The difference in the two models is basically in the fall-off at high frequencies. A simple revision of Haskell's model produces waveforms and spectra nearly identical to ones from Mueller and Murphy's model. This revision requires velocity waveforms to have a rise time of extremely short duration at the elastic boundary, a premise validated by actual near-field measurements.

Waveforms are derived from the revised Haskell model and the Mueller and Murphy model and illustrated for pressure at the elastic boundary, reduced displacement potential at the elastic boundary, and far-field displacement. Corresponding spectra are derived and illustrated.

1. Synopsis of previous work on source spectra and yield scaling

The response of an infinite homogeneous elastic medium to a pressure function acting on the boundary of a spherical cavity is well known (e.g. Sharpe 1942; Blake 1952). The solution for simple time functions of pressure such as a step or a decaying pulse are straightforward. Recently attempts have been made to model the exact source time function for nuclear detonations with the aid of close-in empirical measurements. Among other reasons, we feel it is imperative to obtain a nearly exact model for the source function so that spectral ratios applied to the short-period band, from 0·2 to 5 cps, can be formed and analysed in an optimum manner for purposes of discrimination between explosions and earthquakes.

Haskell (1967) formulated the source spectrum of an explosion by fitting a parameterized function to actual displacement potential waveforms calculated from measurements just outside the elastic radius of underground nuclear explosions. The proposed function results in a far-field displacement spectrum which is asymptotic as the inverse of the fourth power of frequency (von Seggern & Lambert 1970). This fall-off entails a high-frequency scaling of displacement inversely proportional to the cube root of yield (i.e. large explosions emit *less* high frequency energy than small explosions) and a low-frequency scaling of displacement proportional to yield.

Mueller & Murphy (1971) have formulated a model based on theoretical considerations of the medium response to an explosive source near the surface. The

* Received in original form 1972 May 5

theoretical underpinnings are basically those of Sharpe (1942) and Blake (1952). The far-field displacement spectrum from these models is asymptotic as the inverse of the square of frequency for high frequencies. This entails a high-frequency scaling of displacement directly proportional to the cube root of yield, in contrast to Haskell's model. The low-frequency scaling is the same as for Haskell's; that is, displacement is proportional to yield.

The purpose of this report is to compare the two models to data taken from teleseismic recordings of the three Amchitka Island underground tests. A full development of explosion functions will be made after reviewing the data; this will include representations for the pressure and displacement potential at the elastic radius of the explosion, the far-field displacement, and the spectrum of each of these functions. In this report we exclude the effects of the free surface on the theoretical source functions, and for comparison with theory we attempt to remove the free surface effects in the data.

2. Body-wave scaling for Amchitka Island tests

2.1. *Scaling of first motion amplitudes for LONGSHOT, MILROW and CANNIKIN*

We will compare the measured relative amplitudes of the *P*-wave for the three Amchitka Island tests with values calculated from the two theoretical scaling formulas under consideration. The reported yields of the three explosions are: LONGSHOT, 80 kt; MILROW, 1000 kt; CANNIKIN, 5000 kt. In order to avoid the effects of the reflection from the surface, which is delayed approximately a half-second relative to the initial pulse for LONG SHOT (Cohen 1969) and more for the other two shots, we must use the unbiased amplitudes of the initial upward ground motion at the receiver. By measuring this first quarter-cycle of the *P*-wave at several common stations, von Seggern & Lambert (1972) determined the ratio of MILROW to LONGSHOT amplitudes. We have repeated the same procedure with CANNIKIN and MILROW at seven common stations for which data could be obtained at the Seismic Data Laboratory; the measurements are listed in Table 1 along with the MILROW/LONGSHOT ratios reported by von Seggern & Lambert for the same stations plus two additional high-quality stations. The average ratio of CANNIKIN to MILROW amplitude is thus estimated to be 2·56 and MILROW to LONGSHOT to be 6·68.

From Haskell's scaling theory for granite, we can calculate using the displacement spectrum formula as given by von Seggern & Lambert (1970) the relative amplitudes at a frequency of 1 cps. From Haskell's work, one is not able to account for the effects of small changes in medium properties. The granite scaling is used because the Amchitka tests apparently follow the 'hard rock' magnitude-yield scaling at NTS (von Seggern & Lambert 1972). The amplitude ratios are calculated at 1 cps

Table 1

Station	Cannikin / Milrow	Milrow / Longshot
UBO	—	7·94
LAO	2·59	6·89
TFO	2·70	5·59
KN-UT	2·36	7·58
RK-ON	2·63	5·98
CR-NB	2·47	—
HN-ME	2·01	6·10
BE-FL	3·16	—
LC-NM	—	6·71
Average	2·56	6·68
Standard deviation	0·35	0·86

because this agrees fairly well with the period of the first cycle of motion at all the stations for all three shots. There is a slight shift to lower frequencies for increasing yield though. The scaling ratio between two shots in granite at 1 cps is given by:

$$\frac{u_2}{u_1} = \frac{Y_2}{Y_1} \frac{[1+4\pi^2 G^2 Y_2^{\frac{2}{3}} A^2]^{\frac{1}{2}}}{[1+4\pi^2 G^2 Y_1^{\frac{2}{3}} A^2]^{\frac{1}{2}}} \frac{[1+4\pi^2 G^2 Y_1^{\frac{2}{3}}]^{\frac{1}{2}}}{[1+4\pi^2 G^2 Y_2^{\frac{2}{3}}]^{\frac{1}{2}}} \tag{1}$$

where

u = vertical displacement in far-field

Y = yield

G = 0·0185—constant for granite

$A = 1+24B$

B = 0·24—constant for granite.

Calculations using (1) give a ratio of MILROW to LONGSHOT amplitude of 5·60 and a ratio of CANNIKIN to MILROW amplitude of 1·28.

The scaling theory of Mueller & Murphy (1971) involves considerably more terms which must be estimated from available data. Their scaling relation between two shots in different media at different depths at 1 cps is given by:

$$\frac{u_2}{u_1} = \frac{r_{el_2} c_2 \mu_1}{r_{el_1} c_1 \mu_2} \cdot \left[\frac{\varepsilon_1^2+4\pi^2}{\varepsilon_2^2+4\pi^2}\right]^{\frac{1}{2}} \cdot \left[\frac{4\pi^2 p_{0s_2}^2+\varepsilon_2^2 p_{0c_2}^2}{4\pi^2 p_{0s_1}^2+\varepsilon_1^2 p_{0c_1}^2}\right]^{\frac{1}{2}}$$

$$\left[\frac{16\pi^4 \beta_1^2+(1-2\beta_1)4\pi^2 \omega_{0_1}^2+\omega_{0_1}^4}{16\pi^4 \beta_2^2+(1-2\beta_2)4\pi^2 \omega_{0_2}^2+\omega_{0_2}^4}\right]^{\frac{1}{2}} \tag{2}$$

where

r_{el} = elastic radius

c = compressional-wave velocity

μ = rigidity modulus

$\omega_0 = c/r_{el}$

$\beta = (\lambda+2\mu)/4\mu$ (λ is Lamé's constant)

$\varepsilon = \alpha\omega_0$ (α being approximately 2 for granite)

$p_{0s} = 1{\cdot}5\,\rho g h$ (ρ is density, g is gravitational acceleration, and h is depth)

$p_{0c} = (4\mu/3)\,(r_c/r_{el})^3$ (r_c is final cavity radius).

The value p_{0s} is the initial pressure, and p_{0c} is the residual pressure at large t. Several assumptions must be made now. We first assume $\lambda = 2\mu$ thus making $\beta = 1$. (Letting $\lambda = \mu$ instead would not change the scaling significantly.) We then utilize the r_{el} and r_c scaling relations of Mueller & Murphy (1971, equations (15) and (19)) in a rhyolite medium; the two radii scale approximately as the cube root of yield, with dependence on depth and elastic parameters also. For the LONGSHOT site, at the detonation depth of 0·70 km we use $c = 3{\cdot}5\ \mathrm{km\,s^{-1}}$ as indicated by the velocity log at the LONGSHOT site (U.S. Army Engineers 1965). For the MILROW site, at the detonation depth of 1·22 km we use $c = 4{\cdot}0\ \mathrm{km\,s^{-1}}$ as indicated by the velocity log prepared by Snyder (1969). We do not as yet know the velocity at the CANNIKIN site; but using an accepted velocity–depth law of $c = c_0+a(h-h_0)$ where c is the

Table 2

	Milrow Longshot		Cannikin Milrow	
	Amplitude ratio	Magnitude difference	Amplitude ratio	Magnitude difference
Measured data	6·68	0·82	2·56	0·41
Haskell's Model	5·60	0·75	1·28	0·11
Mueller & Murphy's Model	4·93	0·69	2·23	0·35

estimated velocity for the CANNIKIN detonation point of 1·81 km, c_0 is the MILROW velocity of 4·0 km s^{-1}, and $a = 1$ km s^{-1} km^{-1}, we obtain a velocity of 4·6 km s^{-1} for CANNIKIN. Using the relation $\lambda = 2\mu$, we can calculate the rigidity moduli for all three sites; LONGSHOT, 7·4; MILROW, 10·6; CANNIKIN, 12·7. To calculate the peak pressures, p_{0s}, we use $\rho = 2{\cdot}4$ g cm^{-3} at all three sites as indicated by the fairly constant density–depth profile at the LONGSHOT site (U.S. Army Engineers 1965). The remainder of the parameters in (2), ε, ω_0, and p_{0c}, can now be calculated. Application of (2) then to the three tests results in predicted amplitude ratios of MILROW to LONGSHOT of 4·93 and of CANNIKIN to MILROW of 2·23.

Table 2 summarizes the observed and calculated amplitude ratios. Both the scaling relations of Haskell and Mueller & Murphy agree with the actual MILROW to LONGSHOT amplitudes quite well. For CANNIKIN to MILROW, however, Haskell's scaling is significantly in error while that of Mueller and Murphy agrees very well with the data.

For three reasons the above comparisons cannot be entirely convincing in supporting Mueller and Murphy's scaling relation over Haskell's. Firstly, the change in the spectral shape with increasing yield in conjunction with the frequency response of the short-period recording systems may distort the measured relative amplitudes; however, we have estimated that this effect cannot be more than approximately 0·1 for the magnitude difference. Secondly, the number of assumptions and estimations required in applying Mueller & Murphy's scaling relation calls for considerable error limits on its results. Thirdly, Haskell's theory allows for no comparison between shots at different depths and in media other than the four which he examined and is therefore not a general scaling theory, although depth dependency could easily be incorporated using Mueller and Murphy's depth scaling relations, in particular, that for r_{el}.

2.2. *P-wave spectral ratios at RK–ON*

To reinforce the results of the comparison using initial *P*-wave amplitude data, we will examine the entire short-period band of the recorded *P*-waves from CANNIKIN, MILROW, and LONGSHOT and compare this with spectral calculations from the two proposed scaling relations.

Specifically, we examine the spectra of LONGSHOT and MILROW *P* waves at RK–ON as shown by von Seggern & Lambert (1972). RK–ON was chosen among many stations because the signal is above the noise out to 6 cps even for LONGSHOT and because the modulation of the spectra by the surface reflection is nearly ideally exemplified in both cases. We can remove the effect of the surface reflection when we merely smooth over these modulations by connecting adjacent spectral peaks with straight lines to get the spectra shown in Fig. 1. The CANNIKIN *P*-wave spectrum was then formed in the same manner and is also shown in Fig. 1. All the spectra were computed from the first three or four seconds of signal. The unexpected rise in the CANNIKIN spectra at high frequencies is due to the recording system which had been changed for the CANNIKIN event at RK–ON; this noise is evident preceding the CANNIKIN signal. From these smoothed spectra, we calculate

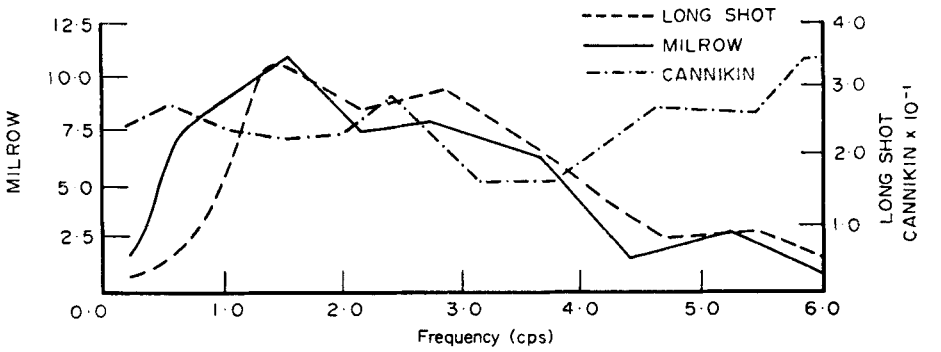

FIG. 1. RK-ON smoothed acceleration spectra for LONGSHOT, MILROW, and CANNIKIN.

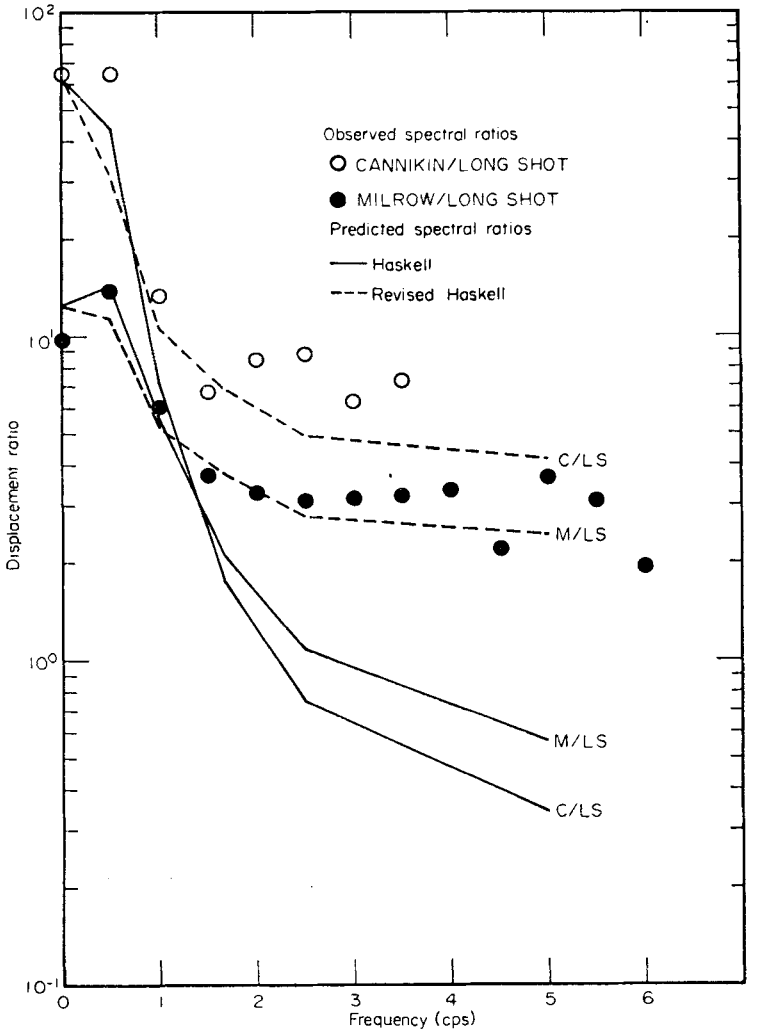

FIG. 2. Theoretical and observed displacement ratios for LONGSHOT, MILROW, and CANNIKIN.

amplitude ratios of MILROW to LONGSHOT and CANNIKIN to LONGSHOT at 0·5 cps intervals and plot them as in Fig. 2. Note that we have neglected to calculate empirical CANNIKIN to LONGSHOT ratios beyond 4 cps due to the predominance of noise in this portion of the CANNIKIN spectrum of Fig. 1. In addition, the amplitude ratios at long periods can be obtained from the Rayleigh waves; and we plot these at 0·05 cps in Fig. 2. Using Haskell's scaling relation for 80, 1000 and 5000 kt shots in granite, we compute the spectral ratios shown in Fig. 2. Using a revision of Haskell's model to give a fall-off at high frequencies proportional to the inverse of frequency squared as in Mueller and Murphy's model, we calculate the ratios shown in Fig. 2 which agree remarkably well with the actual data. (This revision will be discussed in the next section, but its form is nearly equivalent to Mueller & Murphy's, and a full extension of equation (2) across the band from 0·5 to 5 cps would produce lines nearly identical to the dotted ones shown in Fig. 2.)

The results of comparing spectral ratios at one station and first motion amplitudes at several stations together affirm the validity of the model of Mueller & Murphy and cast doubt on the validity of Haskell's model. In the next section we will delineate the essential physical differences of the explosive source mechanism as inferred by the two models and develop general forms for representing the source time functions and spectra.

3. Generalized forms for explosive source time functions and spectra

3.1. *Haskell's original formulation*

Haskell (1967) formulated his model by fitting curves of the type

$$\frac{\psi(t)}{\psi(\infty)} = 1-e^{-kt}\left[1+kt+\frac{(kt)^2}{2}+\frac{(kt)^3}{6}-B(kt)^4\right] \tag{3}$$

where $\psi(\infty)$ is the asymptotic value for large t, to reduced displacement potentials calculated from data taken just outside the elastic radius of several underground nuclear detonations. As stated by him, the form of this function was chosen so as to make displacement, velocity, and acceleration functions continuous at $t = 0$ (t is the retarded time referred to the elastic boundary). This entails, as shown by von

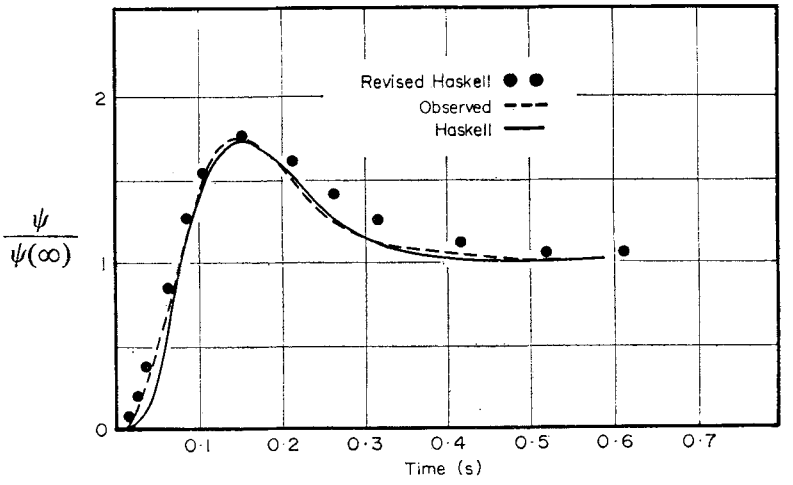

FIG. 3. Observed and analytic displacement potentials for granite (from Haskell 1967) compared to a revised analytic model which assumes a discontinuity in acceleration and velocity at the elastic radius.

Seggern & Lambert (1970), the ω^{-4} dependence at high frequencies for the far-field displacement spectrum. Haskell's curves according to (3) are apparently excellent fits to the data he shows. We reproduce his example for a granite medium in Fig. 3. However, note that at the beginning of the waveform, which is the critical area in relation to the fall-off of the high-frequency portion of the spectrum, his analytic curve has a slope significantly less than the real slope. We feel that Haskell's requirement of continuous acceleration and velocity at the elastic radius is physically too restrictive, and therefore we can safely assume the more idealized case where acceleration and even velocity are discontinuous at the elastic boundary of the medium surrounding the explosion. These may not be exact discontinuities, but the jump should occur in a time span which is nearly instantaneous relative to the frequency band under consideration. Numerous particle velocity recordings outside the elastic boundary of underground nuclear shots (e.g. GASBUGGY in Perret 1972) show that the velocity takes a large initial jump in a time span on the order of 0·01 s.

3.2. *Revision of Haskell's model*

By removing the quartic and cubic terms from (3), we remove the constraints of continuous acceleration and velocity in the near field. Then we propose a source model by fitting the function

$$\frac{\psi(t)}{\psi(\infty)} = 1-e^{-kt}[1+kt-B(kt)^2] \tag{4}$$

to the same data as used by Haskell. Values of k and B will then differ from those published by Haskell using (3). For the granite case in particular, we get new values of $k = 16{\cdot}8$ at 5 kt and $B = 2{\cdot}04$ by requiring that (4) fit the peak of the measured potential and the asymptotic long-time value $\psi(\infty)$. Several calculated points of this curve are shown in Fig. 3.

The reduced displacement potential (4) and the pressure function on the elastic radius are related by (Rodean 1971, equation (4.17)):

$$\frac{r_{el}}{\rho\psi(\infty)}\sigma(t) = \frac{d^2[\psi(t)/\psi(\infty)]}{dt^2} + \frac{4b^2}{cr_{el}}\frac{d[\psi(t)/\psi(\infty)]}{dt} + \frac{4b^2}{r_{el}^2}\frac{\psi(t)}{\psi(\infty)}. \tag{5}$$

where b is the shear velocity. Using (4) in (5), we obtain

$$\frac{r_{el}^3}{4\rho b^2\psi(\infty)}\sigma(t) = e^{-kt}\left\{\left[\frac{c^2\gamma^2}{4b^2}-\gamma+1\right]B(kt)^2 + \left[-\frac{c^2\gamma^2}{4b^2}(4B+1)+\gamma A'-1\right]kt+\frac{c^2\gamma^2}{4b^2}A'-1\right\}+1 \tag{6}$$

where $A' = 2B+1$, and we have assumed $k = \gamma c/r_{el}$. By equation 4.22 of Rodean (1971), we have for ω small in the frequency domain or t large in the time domain:

$$\psi(\infty) = \frac{r_{el}^3 p_{0c}}{4\rho b^2}. \tag{7}$$

Applying this relation to (6) results in:

$$\frac{1}{p_{0c}}\sigma(t) = e^{-kt}\left\{\left[\frac{c^2\gamma^2}{4b^2} - \gamma + 1\right]B(kt)^2 + \left[-\frac{c^2\gamma^2}{4b^2}(4B+1) + \gamma A' - 1\right]kt + \frac{c^2\gamma^2}{4b^2}A' - 1\right\} + 1. \quad (8)$$

We desire an expression for the far-field displacement also; this can be derived from the reduced displacement potential (4) if we employ this relation (Rodean 1971, equation (4.16)):

$$\frac{u(t)}{\psi(\infty)} = \left\{\frac{1}{cr}\frac{d[\psi(t)/\psi(\infty)]}{dt} + \frac{1}{r^2}\frac{\psi(t)}{\psi(\infty)}\right\}. \quad (9)$$

For the far-field displacement, we ignore the second term in (9) and thus have

$$\frac{cr}{\psi(\infty)}u(t) = \frac{d[\psi(t)/\psi(\infty)]}{dt}. \quad (10)$$

Substituting (4) in (10) then gives

$$\frac{cr}{\psi(\infty)}u(t) = -k^2 t\, e^{-kt}(Bkt - A'). \quad (11)$$

Equations (8), (4), and (11) give the pressure, reduced displacement potential, and far-field displacement waveforms. The parameter k is medium dependent; and

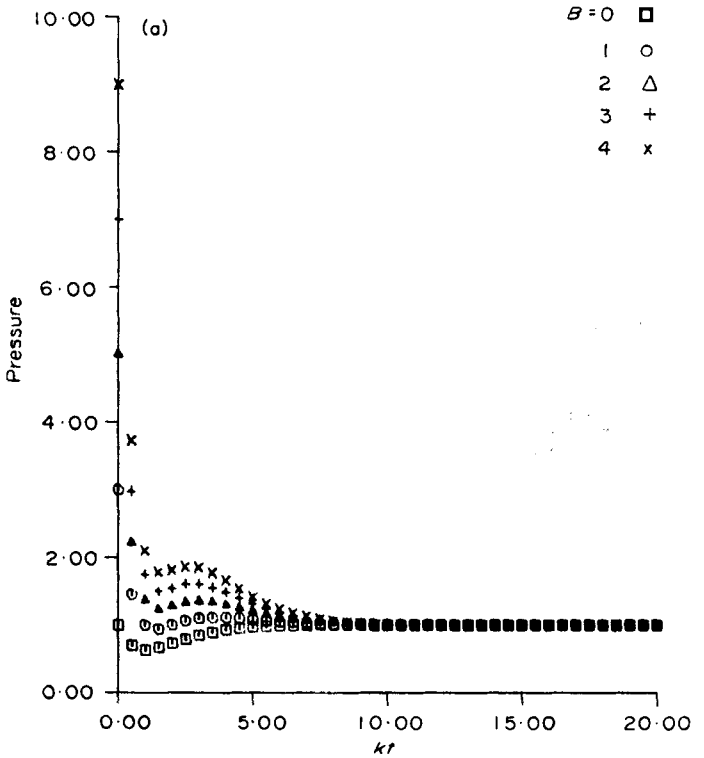

FIG. 4(a)

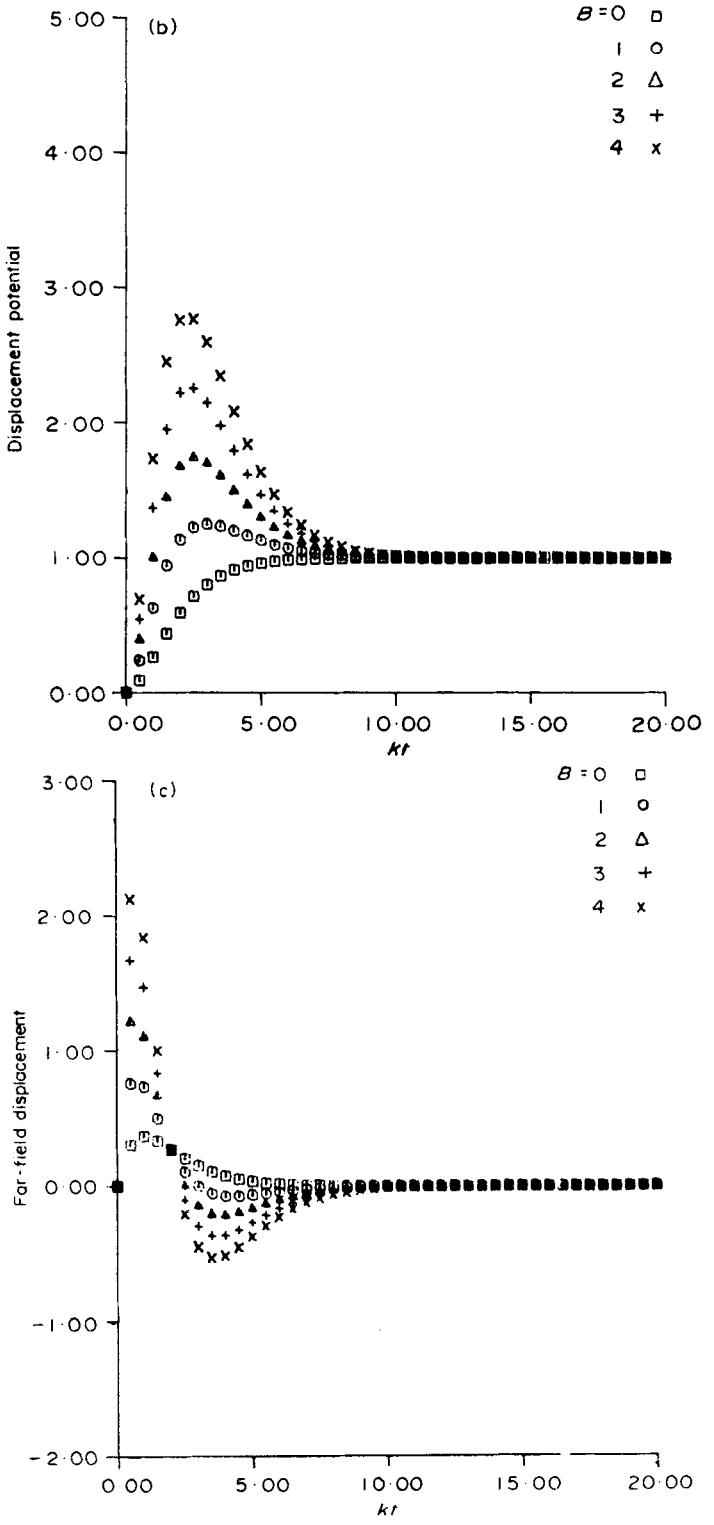

FIG. 4(a). Pressure waveforms at the elastic boundary calculated from revised Haskell's model. (b) Reduced displacement potential waveforms at the elastic boundary calculated from revised Haskell's model. (c) Far-field displacement waveforms calculated from revised Haskell's model.

we assume, as did Haskell, that it scales as the inverse cube root of the yield. B is a medium-dependent parameter which defines the amount of overshoot in the reduced displacement potential wave-form. In Fig. 4(a), (b) and (c) we show (8), (4), and (11), respectively, as a function of the dimensionless parameter kt for five values of B: 0, 1, 2, 3, and 4. We have set $\gamma = 1$ and $b/c = \frac{1}{2}$ in equations (8) and (4). The case $B = 2$ for the reduced potentials in Fig. 4(b) closely corresponds with the fit of (4) to the granite data of Haskell in Fig. 3 when B was calculated to be 2·04. It appears that equation (4) then can fit observed potentials as well as Haskell's original function, equation (3). Not only does the elimination of quartic and cubic terms from Haskell's function produce a more physically satisfying function as explained above, but it does so without suffering any significant loss of fitting capability.

Spectra of the above three functions for pressure at the elastic radius, reduced potential at this radius, and far-field displacement can be derived. Only the far-field displacement spectrum should be of interest though; taking the Fourier transform of (11), its form is:

$$\frac{cr}{\psi(\infty)}\,|u(\omega)| = \frac{[A'^2(\omega/k)^2+1]^{\frac{1}{2}}}{[(\omega/k)^2+1]^{\frac{3}{2}}}. \tag{12}$$

Equation (12) is plotted in Fig. 4 as a function of the dimensionless parameter ω/k for B values of 0, 1, 2, 3 and 4. Note that the required ω^{-2} fall-off of the displacement spectra at high frequencies is present and that the overshoot in the displacement spectra is proportional to B.

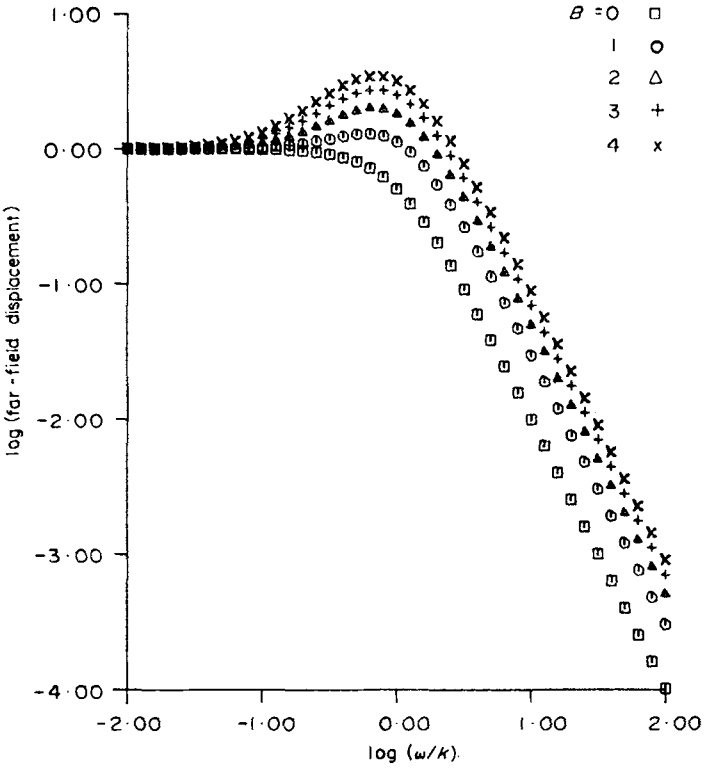

FIG. 5. Far-field displacement spectra calculated from revised Haskell's model.

3.3. *Mueller & Murphy's formulation*

Mueller & Murphy (1971) take a slightly different approach in deriving scaling relations. They assume the arbitrary form

$$\frac{1}{p_{0c}}\sigma(t) = p\exp(-\alpha\omega_0 t)+1 \tag{13}$$

for the pressure at the elastic radius where $p = p_0/p_{0c}$ and $p_0 = p_{0s}-p_{0c}$ (p_{0s} and p_{0c} are defined as for equation (2)) whereas Haskell began with an arbitrary form for reduced displacement potential. To derive the reduced displacement potential from the pressure function, we transform (13) into the frequency domain, apply equation (4.19) in Rodean, and inverse transform back to the time domain to get the reduced potential function. Inverse transforms #0·011 and #0·101 in Nixon (1960) are employed with the damping coefficient (b/c in this case) set to one-half. The reduction is straightforward, but tedious, and we give only the final result:

$$\frac{\psi(t)}{\psi(\infty)} = \exp(-\omega_0 t/2)\left\{0{\cdot}577\left[\frac{p(2\alpha-1)}{1-\alpha+\alpha^2}-1\right]\sin(0{\cdot}866\omega_0 t)\right.$$

$$\left.-\left[\frac{p}{1-\alpha+\alpha^2}+1\right]\cos(0{\cdot}866\omega_0 t)\right\}+\frac{p}{1-\alpha+\alpha^2}\exp(-\alpha\omega_0 t)+1. \tag{14}$$

The far-field displacement is obtained by use of (10) as before:

$$\frac{cr}{\psi(\infty)}u(t) = \omega_0\exp(-\omega_0 t/2)\left\{\frac{p\alpha}{1-\alpha+\alpha^2}\cos(0{\cdot}866\omega_0 t)\right.$$

$$\left.-1{\cdot}154\left[\frac{p(\alpha/2-1)}{1-\alpha+\alpha^2}-1\right]\sin(0{\cdot}866\omega_0 t)\right\} \tag{15}$$

$$-\frac{\omega_0 p\alpha}{1-\alpha+\alpha^2}\exp(-\alpha\omega_0 t).$$

The pressure (13) could be plotted as a function of the dimensionless parameter $\alpha\omega_0 t$, but the reduced displacement potential (14) and the far-field displacement (15) cannot. Thus in fitting observed reduced potentials, Mueller & Murphy's formulation requires the additional parameter α to be estimated. The parameter $\alpha\omega_0$ corresponds to k in Haskell's formulation, and the parameter p here corresponds to his $2B$. In Fig. 6(a), (b) and (c), we show the plots of (13), (14) and (15), respectively, as a function of $\omega_0 t$ for $\alpha = 2$ when p is assigned values of 0, 2, 4, 6 and 8. Several other values of α were used, but $\alpha = 2$ is the value Mueller & Murphy suggest for rhyolite, which is compositionally close to granite. For $\alpha = 2$ and $p = 4$ in the reduced potentials of Fig. 6(b), the curve closely corresponds in amplitude to the revised Haskell potential in Fig. 4(b) when B is taken to be 2, approximately the value we obtained when fitting (4) to the granite data shown in Fig. 3. This shows the analogy of p to $2B$.

The far-field displacement spectrum follows from (15) by Fourier transformation:

$$\frac{cr}{\psi(\infty)}|u(\omega)| = \left[\frac{(p+1)^2(\omega/\omega_0)^2+\alpha^2}{(\omega/\omega_0)^2+\alpha^2}\right]^{\frac{1}{2}}\cdot[1-(\omega/\omega_0)^2+(\omega/\omega_0)^4]^{-\frac{1}{2}}. \tag{16}$$

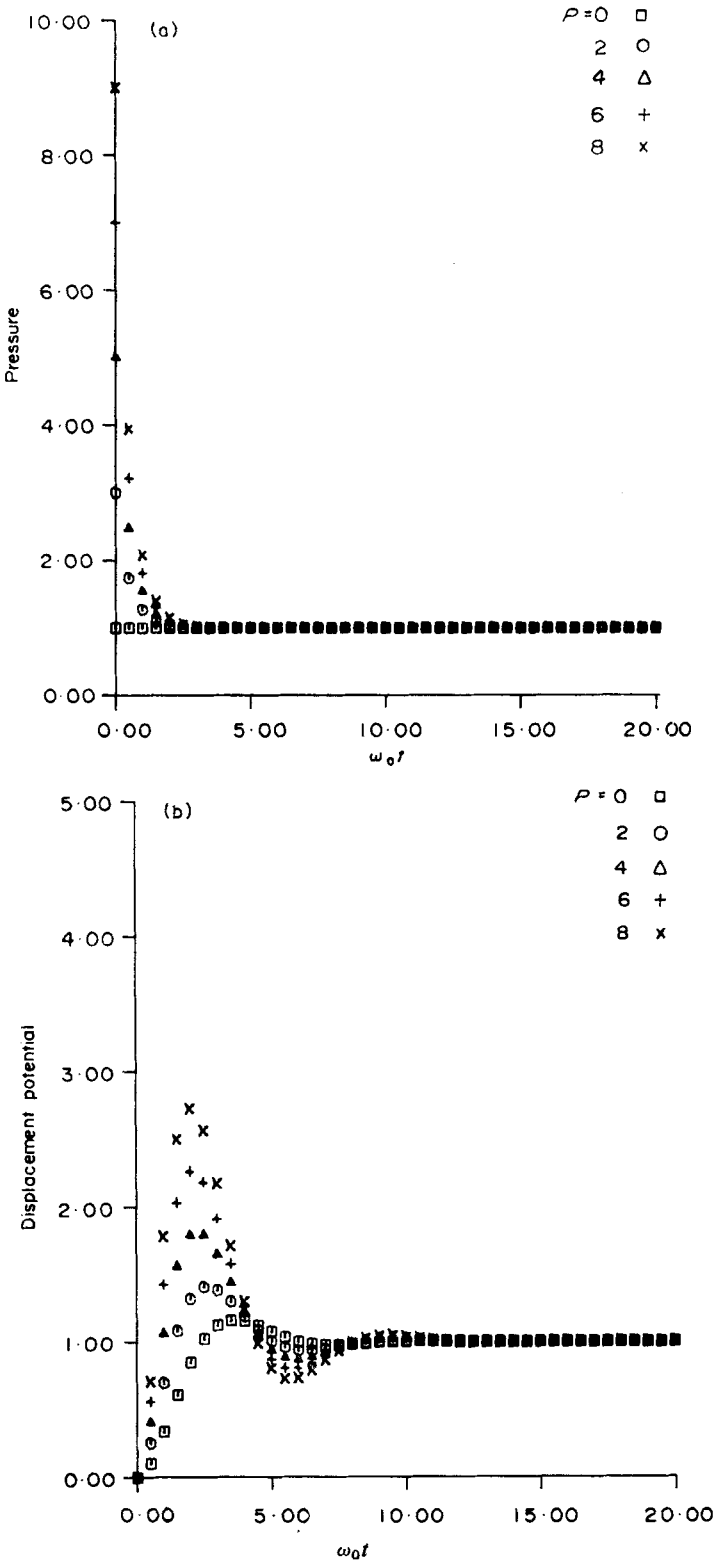

FIG. 6(a) and (b)

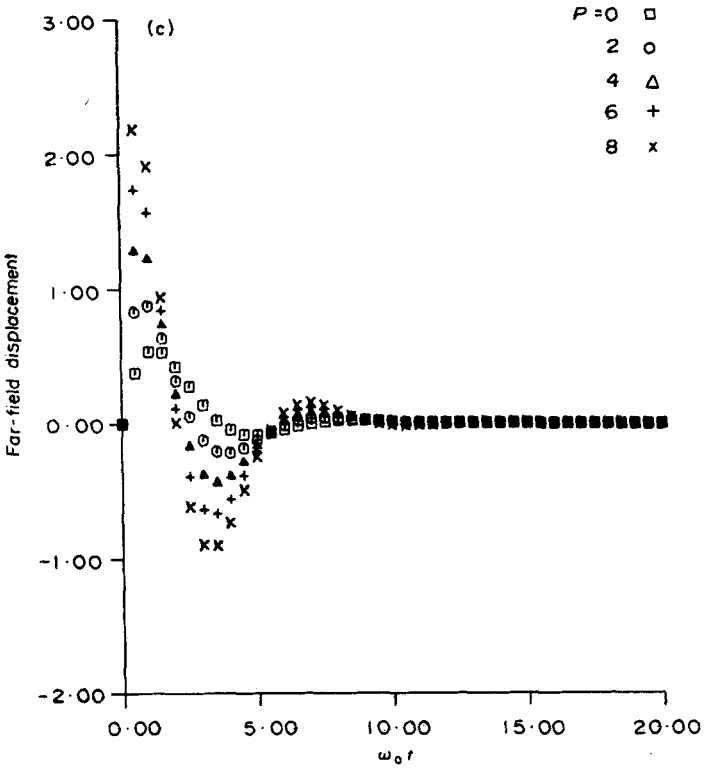

FIG. 6(a). Pressure waveforms at the elastic boundary calculated from Mueller & Murphy's model. (b) Reduced displacement potential waveforms at the elastic boundary calculated from Mueller & Murphy's model. (c) Far-field displacement waveforms at the elastic boundary calculated from Mueller & Murphy's model.

In Fig. 7 we plot (16) for $\alpha = 2$ with p set from 0 to 8 again. Comparison of Fig. 7 with $p = 4$ to Fig. 5 with $B = 2$ shows the similarity of the revised Haskell model and the Mueller & Murphy model for a granite–rhyolite medium. This similarity is evident in the spectral formulas if we let $k = \gamma\omega_0$ in (12) to obtain:

$$\frac{cr}{\psi(\infty)}|u(\omega)| = \left[\frac{A'^2(\omega/\omega_0)^2+\gamma^2}{(\omega/\omega_0)^2+\gamma^2}\right]^{\frac{1}{2}} \cdot [1+2(\omega/\gamma\omega_0)^2+(\omega/\gamma\omega_0)^4]^{-\frac{1}{2}} \qquad (17)$$

and compare this with (16). For ω small (16) and (17) give equivalent spectral densities when $p = 2B$; but for ω large the revised Haskell spectrum would be a factor of γ^2 larger for a given ω/ω_0 when $p = 2B$. If, however, we assume $\gamma = \alpha/2$, then this factor is exactly one for the granite case and the predicted far-field displacement spectra are equivalent for the two models. That a value of $\gamma = 1$ is indeed correct for granite in the revised Haskell model follows from the definition $\gamma = r_{el}\,k/c$ when appropriate values are substituted. A value of $r_{el} = 0{\cdot}37$ km is taken for LONGSHOT (Mueller & Murphy 1971, equation (15)); a value of 3·5 is taken for c as stated earlier in this paper; and k, 16·8 for a 5 kt explosion at 0·29 km (HARDHAT), is scaled to 80 kt and 0·70 km for LONGSHOT to get $k = 9{\cdot}6$ (Mueller & Murphy 1971, equation (14)). These values result in $\gamma = 1{\cdot}02$, approximately the desired value.

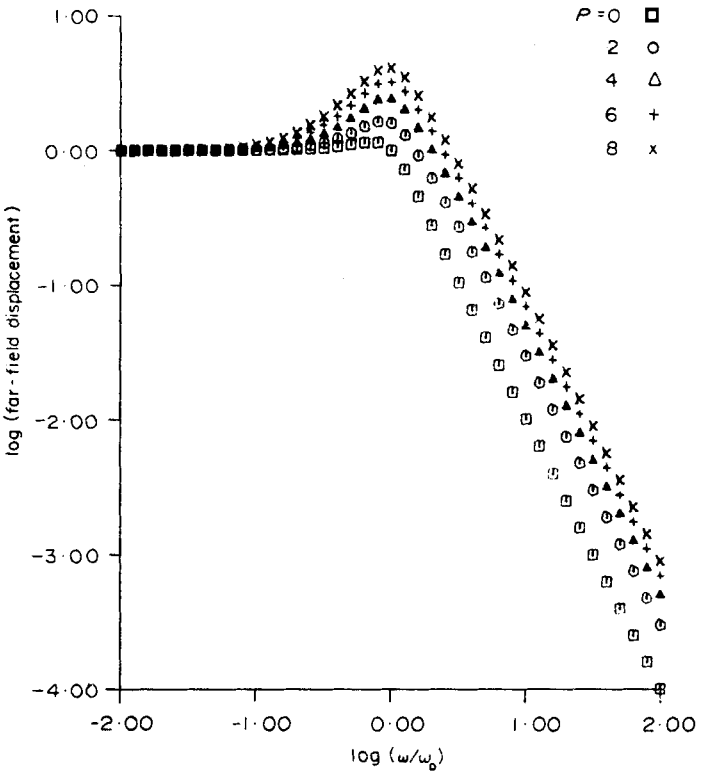

FIG. 7. Far-field displacement spectra calculated from Mueller & Murphy's model.

4. Discussion

Using teleseismic data, we have shown that a model for the explosion source function which entails a far-field displacement spectrum that is proportional to ω^{-2} at high frequencies is the proper choice. Mueller & Murphy (1971) have already verified this model using near-field data. Haskell's requirement that acceleration and velocity be continuous at the elastic boundary around the explosion is unnecessary; they certainly can be considered as discontinuous for any part of the spectrum capable of being measured teleseismically. We mention that the ω^{-2} dependence at high frequencies is characteristic of earthquake models also (Aki 1967; Brune 1970).

We have revised Haskell's formulation to obtain an ω^{-2} model and found that the fit to observed potentials is apparently as good as with his original ω^{-4} model. We have used Mueller & Murphy's formulation for the pressure function at the elastic radius to derive reduced potential and far-field displacement waveforms. Waveforms and spectra for the two ω^{-2} models are similar. Observed waveforms can be fit by adjusting the parameters in either model. Especially important is estimation of the parameter p (or B) which is the ratio of the overshoot pressure p_0 to the residual pressure p_{0c} at the elastic boundary. This value controls the peak in the far-field spectra and affects spectral ratios in the band around 1 cps. These pressures can be estimated using the relations in equation (2) as taken from Mueller & Murphy. The parameter ω_0 also controls the spectral shape near 1 cps, but its effect is predictable since $\omega_0 = c/r_{el}$ and r_{el} scales as the cube root of yield when detonation depths are equal (Mueller & Murphy 1971).

Acknowledgments

This work was supported by the Advanced Research Projects Agency and monitored by the Air Force Technical Applications Center under Contract F33657–72–C–0009.

Seismic Data Laboratory,
Teledyne Geotech,
314 *Montgomery Street,*
Alexandria, Virginia.

References

Aki, Keiiti, 1967. Scaling law of seismic spectrum, *J. geophys. Res.*, **72,** 1217.

Blake, F. G., 1952. Spherical wave propagation in solid media, *J. acoust. Soc. Am.*, **24,** 211.

Brune, James N., 1970. Tectonic stress and the spectra of seismic shear waves from earthquakes, *J. geophys. Res.*, **75,** 4997.

Cohen, T. J., 1970. Source-depth determinations using spectral, pseudo-auto-correlation, and cepstral analysis. *Geophys. J. R. astr. Soc.*, **20,** 223.

Haskell, N. A., 1967. Analytic approximation for the elastic radiation from a contained underground explosion, *J. geophys. Res.*, **72,** 2583.

Mueller, Richard A. & Murphy, John R., 1971. Seismic characteristics of underground nuclear detonations: Part I, Seismic scaling law of underground detonations, *Bull. seism. Soc. Am.*, **61,** 1675.

Nixon, Floyd E., 1960. *Handbook of Laplace Transformation*, Prentice-Hall, Inc., Englewood Cliffs, New Jersey.

Perret, William R., 1972. Gasbuggy seismic source measurements, *Geophysics*, **37,** 301.

Rodean, Howard C., 1971. *Nuclear-Explosion Seismology.* U.S. Atomic Energy Commission, Division of Technical Information.

Seggern, David von & Lambert, D. G., 1970. Theoretical and observed Rayleigh-wave spectra for explosions and earthquakes, *J. geophys. Res.*, **75,** 7382.

Seggern, D. H. von & Lambert, D. G., 1972. Analysis of teleseismic data for the nuclear explosion MILROW, *Seismic Data Laboratory Report No.* 258, Teledyne Geotech (AD 743–072).

Sharpe, J. A., 1942. The production of elastic waves by explosion pressures: I, Theory and empirical field observations, *Geophysics.*, **7,** 144.

Snyder, Richard P., 1969. Preliminary lithologic log of drill hole UAe-2 from 0 to 3,580 feet, Amchitka Island, Alaska. *United States Geological Survey Report No.* 474–52 (Amchitka-10).

United States Army Engineer District, Alaska, and United States Geological Survey, 1965. Project LONGSHOT, Amchitka Island, Alaska: *Geologic and hydrologic investigations* (Phase I).